Isotopic composition of stratospheric water vapor: Implications for transport

David G. Johnson,[1] Kenneth W. Jucks, Wesley A. Traub, and Kelly V. Chance
Harvard-Smithsonian Center for Astrophysics, Cambridge, Massachusetts

Abstract

We develop a series of models of transport in the upper tropical troposphere in order to explain the observed abundance and isotopic composition of stratospheric water vapor. We start with the Rayleigh fractionation process and add the effects of mixing and recirculation of stratospheric air through the upper troposphere. We compare our measurements with model calculations for a range of input parameters and find that the observations are best explained by a model that mixes vapor from roughly 11 km (carried aloft either as condensate or through radiative heating and uplift) with air that has been dehydrated (in a large convective system) to a mixing ratio substantially below the saturation mixing ratio of the mean tropical tropopause. The result is that while most of the moisture comes from convective outflow near 11 km, most of the air in the upper troposphere consists of dehydrated air from convective systems with cloud top temperatures below that of the mean tropical tropopause. We also find that the water vapor mixing ratio in the stratosphere is determined not only by the temperature of the tropical tropopause but also by the relative importance of radiative heating, recirculation of stratospheric air, and deep convection in supplying air to the upper troposphere. Our results show that water vapor isotope ratios are a powerful diagnostic tool for testing the results of general circulation models.

[1] Now at NASA Langley Research Center, Hampton, Virginia.

1. Introduction

Measurements of stratospheric water vapor have long been a tool for constructing models of large-scale motion, starting with the idea that air enters the stratosphere primarily by crossing the tropical tropopause [*Brewer*, 1949], possibly in limited geographic areas [*Newell and Gould-Stewart*, 1981]. Measurements of water vapor have also been used to show that air can enter the lowermost stratosphere by crossing the extratropical tropopause through isentropic transport from the tropical upper troposphere [*Dessler et al.*, 1995]. More recently, measurements of the isotopic composition of stratospheric water vapor have shown the inadequacy of simple models in which air is steadily dehydrated as it cools during ascent from the surface to the tropical tropopause [*Moyer et al.*, 1996, *Keith*, 2000].

In the following sections we develop several models for estimating the isotopic composition and abundance of water vapor in the upper tropical troposphere and lower stratosphere. We start with a simple Rayleigh fractionation process and then consider the effects of mixing and recirculation of stratospheric air through the upper troposphere. We highlight the dependence of model results on a limited number of free parameters by deriving approximate analytical expressions rather than relying on numerical models. Finally, we compare the model calculations with measurements to constrain the model parameters.

2. Isotopic Standards

Measurements of an isotope ratio R, such as $R = [\mathrm{HDO}]/[\mathrm{H_2O}]$, where $[X]$ signifies the volume mixing ratio of X, are typically reported relative to a standard ratio R_0, often using δ notation:

$$\delta(‰) \equiv 1000(R/R_0 - 1)\,.$$

We use standard mean ocean water isotope ratios for R_0 and adopt the values 2.0052×10^{-3} and 1.5576×10^{-4} for $[^{18}\mathrm{O}]/[^{16}\mathrm{O}]$ and and $[\mathrm{D}]/[\mathrm{H}]$, respectively [*De Bièvre et al.*, 1984]. When calculating δ, we assume a standard ratio of $2(1.5576 \times 10^{-4})$ for $[\mathrm{HDO}]/[\mathrm{H_2O}]$.

In this paper we will consider only singly substituted isotopomers, since the natural abundance of $\mathrm{H_2O}$ molecules with multiple isotope substitutions is low enough to be ignored in the present discussion. In the following sections we will use Q to signify $^{18}\mathrm{O}$ and O to signify $^{16}\mathrm{O}$.

3. Transport Models

In the following subsections we develop models for calculating the relationships between $[\mathrm{H_2O}]$, δQ, and δD that result from the vapor pressure isotope effect. The models consider condensation, evaporation, and mixing, but they do not include photochemistry (see *Johnson et al.* [this issue] and *Irion et al.* [1996] for a description of the photochemical modeling of water vapor isotope ratios) and are only appropriate for describing tropospheric processes. In section 4. we use the models to interpret the measurements presented by *Johnson et al.* [this issue].

3.1. Rayleigh Fractionation

We start by constructing a model that only considers Rayleigh fractionation, defined as the depletion of heavy isotopes in the gas phase, caused by advective uplift and subsequent cooling of a saturated air parcel and the formation of condensate enriched in heavy isotopes, in the limit where the condensate is removed as soon as it forms [*Dansgaard*, 1964, *Smith*, 1992]. The specific heat (but not latent heat) of the condensate is neglected, so the process is pseudoadiabatic, and removal of the condensate allows us to ignore isotope exchange between vapor and condensate as the temperature changes during advection. We make the additional assumption that the water vapor mixing ratio is small, so that dehydration does not significantly change the total number density, and derive differential equations for pressure, water vapor mixing ratio, and isotope ratio as functions of temperature.

We first consider $d\ln P/dT$. We assume that air behaves like an ideal gas, so that $m = PV/R_aT$, where m, P, V, T, and R_a are the mass, pressure, volume, temperature, and gas constant for a parcel of air, respectively. We assume that the partial pressure of water vapor is the saturation vapor pressure at the local temperature T, given by the function $e_s(T)$. The mass of water vapor in an air parcel, m_e, is given by

$$m_e = me_sR_a/PR_e\,, \tag{1}$$

where R_e is the gas constant for water vapor. It follows from conservation of energy and the first law of thermodynamics that $-Ldm_e = mc_vdT + PdV$, where L and c_v are the latent heat of vaporization for water and specific heat of air at constant volume, respectively. The first term is the heat released by the condensation of a mass of water vapor equal to dm_e, the second term is the change in internal energy, and the third term is the work done by the expanding gas. Using the ideal gas law to evaluate dV/dT, we derive

$$-Ldm_e/dT = m(c_p - R_aTdP/PdT)\,, \tag{2}$$

where c_p is the specific heat at constant pressure and we have used the relationship $c_v + R_a = c_p$. We combine (1) and (2) and derive

$$d\ln P/dT = (c_p + R_a L de_s/R_e P dT) \\ /(R_a T + R_a L/R_e P) \,. \quad (3)$$

The expression for $d\ln X/dT$, where X is the water vapor mixing ratio, follows from the assumption that $X = e_s(T)/P$:

$$d\ln X/dT = d\ln e_s/dT - d\ln P/dT \,. \quad (4)$$

We now derive an expression for $d\ln R/dT$, where $R \equiv Y/X$ and Y is the mixing ratio of HDO or H_2Q. For water vapor in isotopic equilibrium with condensate, $R_c/R_v = \alpha(T)$, where R_c is the isotope ratio in the condensate, R_v is the isotope ratio in the vapor, and α is the isotopic fractionation factor, which is a function of temperature, isotope, and condensate phase (liquid or solid) [*Jancso and Van Hook*, 1974]. If we start with an air parcel with an initial isotope ratio R and then form condensate with an isotope ratio that satisfies the requirement $R_c = \alpha R_v$, it follows from conservation of molecule number that the change in isotope ratio for the vapor is given by

$$d\ln R/dT = (\alpha - 1) d\ln X/dT \,. \quad (5)$$

Given initial values for P, X, R, and T, as well as the functions $e_s(T)$ and $\alpha(T)$, we calculate the functions $P(T)$, $X(T)$, $\delta D(T)$, and $\delta Q(T)$ by numerically integrating (3)–(5) using a fourth-order Runge-Kutta algorithm [*Press et al.*, 1992] and then calculating δ from R. We adopt the following numerical values for fundamental constants: $R_a = 287.04\ \mathrm{J\,kg^{-1}K^{-1}}$, $R_e = 18R_a/28.96$, and $c_p = 7R_a/2$ [*Smithsonian Institution*, 1951]. We assume that latent heat is independent of temperature and that the latent heats of vaporization and sublimation are $2.5 \times 10^6\ \mathrm{J\,kg^{-1}}$ (resulting in a maximum error of 2.5% between 243 and 303 K) and $2.834 \times 10^6\ \mathrm{J\,kg^{-1}}$ (resulting in a maximum error of 0.5% between 173 and 273 K), respectively [*Smithsonian Institution*, 1951]. In order to simplify this and later calculations, we use the approximation

$$e_s(T) = e_0 \exp(-b/T) \,, \quad (6)$$

where (e_0, b) are given by $(2.5897 \times 10^9\ \mathrm{hPa}, 5431.4\ \mathrm{K})$ and $(3.5753 \times 10^{10}\ \mathrm{hPa}, 6142.0\ \mathrm{K})$ for saturation over water and ice, respectively. The maximum error relative to the Goff-Gratch formulas [*Smithsonian Institution*, 1951] is 2.5% and 0.5% for saturation over water (240–310 K) and ice (180–273 K), respectively. We use the following functional form for $\alpha(T)$:

$$\ln[\alpha(T)] = c_0 + c_1/T + c_2/T^2 \,, \quad (7)$$

where (c_0, c_1, c_2) are given by $(-0.00207, -0.4156\ \mathrm{K}, 1137\ \mathrm{K}^2)$ and $(-0.028224, 11.839\ \mathrm{K}, 0)$ for H_2Q over over water and ice, respectively, and by $(-0.1, 0, 15013\,\mathrm{K}^2)$ and $(-0.0945, 0, 16829\,\mathrm{K}^2)$ for HDO over water and ice, respectively [*Merlivat and Nief*, 1967, *Jancso and Van Hook*, 1974].

We show results in Figure 1 for an initial pressure of 1013 hPa and initial temperatures of 300.5 and 288 K. The initial water vapor mixing ratio and isotope ratios are given by $e_s(T_0)$ and $R_0/\alpha(T_0)$, respectively, where T_0 is the initial temperature. Also shown in Figure 1 are average midlatitude measurements made by the Smithsonian Astrophysical Observatory far-infrared spectrometer (FIRS-2) [*Johnson et al.*, 1995] (the data have been corrected for photochemical aging as described by *Johnson et al.* [this issue]) and comparable measurements made by Atmospheric Trace Molecule Spectroscopy (ATMOS) [*Moyer et al.*, 1996]. The FIRS-2 measurements are sorted into one of three groups before averaging: middle stratosphere ($50 < [N_2O] < 250$ parts per billion by volume (ppbv), potential temperature $(\theta) > 400$ K), lower stratosphere ($[N_2O] > 250$ ppbv, $350 < \theta < 400$ K), and tropopause ($[N_2O] > 250$ ppbv, $\theta < 350$ K; we refer to this region as tropopause and not troposphere because FIRS-2 has never observed air more than 1 km below the local meteorological tropopause). Air in the middle stratosphere is assumed to have entered the stratosphere by crossing the tropical tropopause, while air near the local tropopause is affected by local convection. Air in the lower stratosphere is a mixture of air from the other two regions and may include air that is transported isentropically from the tropical upper troposphere [*Dessler et al.*, 1995].

We also show in Figure 1 the results of an analysis of condensate collected from North Atlantic storm tops and cirrus [*Smith*, 1992] and measurements of water vapor collected at 400 hPa over a range of latitudes [*Zahn et al.*, 1998]. The in situ measurements have been plotted at the local saturation mixing ratio, which should be a good estimate for the cloud top measurements but should be considered an approximate upper limit for the measurements of *Zahn et al.* [1998]. We note that the air may be supersaturated at temperatures below the ice transition, in which case the absolute upper limit would be the saturation vapor pressure over liquid. While FIRS-2 measurements made near the tropopause as well as the cloud top measurements are in reasonable agreement with the pre-

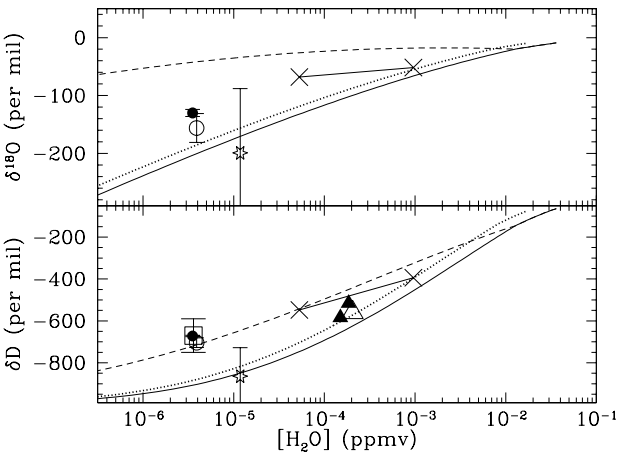

Figure 1. Comparison between measured [H_2O] and δ and calculations with the Rayleigh model discussed in the text. Solid curves show calculation starting at an initial temperature of 300.5 K; dotted curve shows calculation starting at 288 K. Dashed curve shows results when including the kinetic isotope effect for a constant supersaturation of 1.75 over ice (see text). Solid circles, open circles, and stars represent estimates of entry-level composition based on averages of far-infrared spectrometer (FIRS-2) measurements in the midlatitude middle stratosphere, lower stratosphere, and tropopause region, respectively [*Johnson et al.*, this issue]. Large box indicates stratospheric measurement made by Atmospheric Trace Molecule Spectroscopy (ATMOS) [*Moyer et al.*, 1996]. We also show estimates of vapor composition derived from samples of condensate collected from North Atlantic storm tops (solid triangles) and cirrus (open triangle) [*Smith*, 1992] and analysis of tropospheric water vapor samples (curves with crosses) [*Zahn et al.*, 1998]. In situ measurements are shown as a function of the local water vapor saturation mixing ratio, which is an approximate upper limit for the true mixing ratio.

dictions of the Rayleigh model (although the agreement for FIRS-2 measurements may be fortuitous, since measurements in this region have relatively low precision), the FIRS-2 stratospheric measurements and the measurements made by Zahn et al. at low saturation mixing ratios differ significantly from the model. We conclude from the storm top data that the Rayleigh model is appropriate for estimating the isotopic composition of convective outflow, while the other data indicate that the Rayleigh model fails in regions not associated with recent convection.

The discrepancy between stratospheric measurements of δD and what is expected given the extreme dryness of the stratosphere was noted by *Moyer et al.* [1996], who suggested that the difference might be explained by either evaporation of lofted ice or by the kinetic isotope effect (KIE) [*Jouzel and Merlivat*, 1984]. The KIE occurs during ice formation in supersaturated air parcels, and the size of the effect depends on the degree of supersaturation. We also show in Figure 1 the result of including the KIE when the partial pressure of water vapor is held at 175% of the saturation vapor pressure over ice, a physically unrealistic condition that would result in supersaturation over liquid. While these extreme conditions can help explain the observed δD, the results are not consistent with the observed δQ. *Keith* [2000] reached a similar conclusion based on an analysis of an earlier version of the FIRS-2 retrievals presented here; changes in the retrieval are the result of our improvements to the spectral line database as discussed by *Johnson et al.* [this issue].

The inability of the Rayleigh model to explain our measurements in the middle stratosphere, even after considering the KIE, has motivated us to develop a more sophisticated model of transport in the tropical upper troposphere.

3.2. Mixed Model

In this section we develop a model of the tropical troposphere that includes convection, mixing, uplift, and recirculation of stratospheric air through the troposphere. The model is shown schematically in Figure 2. We assume that air enters the stratosphere both through direct injection by large convective systems as proposed by *Newell and Gould-Stewart* [1981] (see, for example, *Vömel et al.* [1995]) and through radiative heating of air in the upper tropical troposphere (see, for example, *Jensen et al.* [1999]). While the model is very simple, we believe that it contains sufficient detail to explore the sensitivity of the abundance and isotopic composition of stratospheric water vapor to different processes occurring in the tropical upper troposphere.

We start by dividing the tropical troposphere into the upper troposphere, defined as the region having a posi-

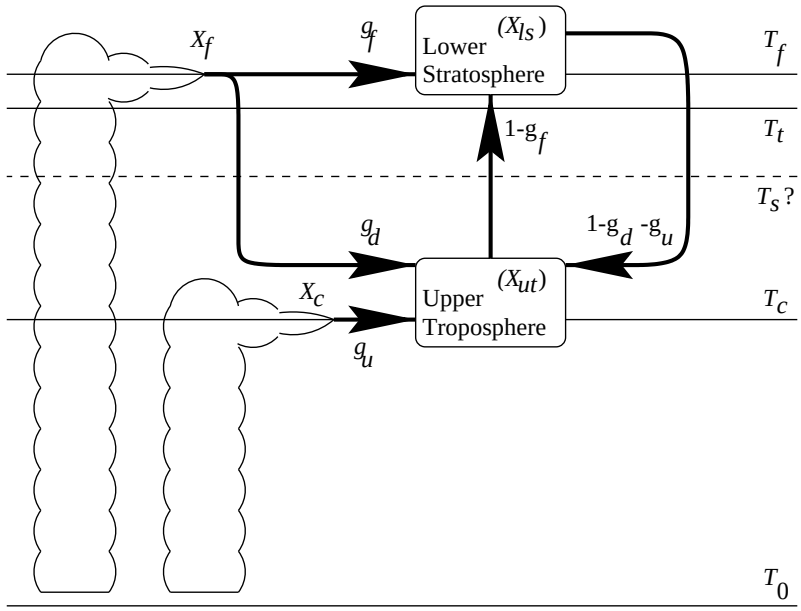

Figure 2. Transport processes included in the model discussed in the text. We show sample volumes in the upper troposphere and lower stratosphere. Stratospheric air is either directly injected by fountain systems (fraction given by g_f) or transported from the upper troposphere. Air in the upper troposphere is a mixture of air from conventional convective systems (g_u), subsided air from fountain systems (g_d), and recirculated stratospheric air ($1 - g_d - g_u$). T_0, T_c, T_t, and T_f are temperatures at the surface, in outflow from conventional systems, at the tropopause, and in outflow from fountain systems, respectively. Water vapor in slowly rising tropospheric air reaches saturation at T_s. If $T_s < T_t$ then the troposphere is unsaturated. Mixing ratios in the lower stratosphere, upper troposphere, fountain outflow, and conventional outflow are indicated by X_{ls}, X_{ut}, X_f, and X_c, respectively.

tive net radiative heating rate, and the lower troposphere, consisting of the rest of the troposphere. We then assume that there are just two categories of convective systems: fountains, which rapidly transport air from near the surface to the tropopause region; and conventional, which transport air from the surface to the base of the upper troposphere. We ignore processes that transport air to lower altitudes, since this air cools and sinks and does not affect the composition of the upper troposphere. While detrainment into the upper troposphere in the real world occurs over a continuous range of altitudes, considering just the two extremes will allow us to estimate a lower limit for the altitude of the fountain top and an upper limit for the base of the upper troposphere, as we show below.

We consider air that enters the stratosphere both through direct injection by fountain systems and through heating and gradual uplift of upper tropospheric air. Upper tropospheric air is considered, in turn, to be a mixture of convective outflow of ice and vapor from conventional systems, subsided air that has been dehydrated in fountain systems, and recirculated stratospheric air. The upper tropospheric air is mixed just once at the base of the upper troposphere (to simplify the model) and then uplifted along the ambient temperature profile. Condensate is removed as necessary to maintain the vapor pressure at saturation over ice. The uplifted air is mixed with fountain air after it crosses the tropopause to determine the final stratospheric composition. For example, consider a tracer with mixing ratios x_{ls}, x_c, and x_f in the lower stratosphere, in outflow from conventional systems, and in outflow from fountain systems, respectively, as shown in Figure 2. Assuming that the tracer does not reach saturation so that we can ignore condensation, x_{ls} is found by solving

$$x_{ls} = g_f x_f + (1-g_f)[g_u x_c + g_d x_f + (1-g_u-g_d)x_{ls}] \,, \quad (8)$$

where g_f is the fraction of stratospheric air that is directly injected by fountain systems, g_u is the fraction of upper tropospheric air consisting of outflow from conventional systems, g_d is the fraction of upper tropospheric air consisting of subsided air dehydrated by fountain systems, and $(1-g_u-g_d)$ is the fraction of upper tropospheric air consisting of recirculated stratospheric air.

Our model is qualitatively similar to the tropical tropopause layer (TTL) model proposed by *Sherwood and Dessler* [2000], with the TTL equivalent to what we define as the upper troposphere. Our model includes recirculation of stratospheric air, not included in the TTL model, and only considers detrainment at two altitudes, while the TTL model includes detrainment throughout the upper troposphere. However, unlike the TTL model, our model is quantitative and provides estimates of the abundance and isotopic composition of stratospheric water vapor that can be compared with observations for a range of input parameters.

We further simplify the model by assuming that the tropospheric lapse rate is constant, making it possible to derive a simple analytical expression for $P(T)$ and allowing us to use either P, T, or z as the independent variable, where z is altitude. We note that, in reality, the lapse rate changes at the tropopause (by definition) and can show considerable variation with altitude in this region. Ignoring changes in the lapse rate will result in errors in the altitude scale near the tropopause as well as small errors in evaluating $P(T)$, but it will not significantly affect our conclusions.

We define $T(z) = T_0 - \Gamma z$, where T_0 and Γ are surface temperature and lapse rate, respectively. Assuming that the atmosphere is in hydrostatic equilibrium, it follows from the ideal gas law that

$$P(T) = P_0 (T/T_0)^a \,, \quad (9)$$

where P_0 is the surface pressure, $a = g/\Gamma R_a$, and $g = 9.80665$ m s^{-2} is the acceleration due to gravity.

Combining (6) and (9), we derive the following expression for saturation mixing ratio X_s as a function of temperature:

$$X_s(T) = (e_0/P_0)(T_0/T)^a \exp(-b/T) \,. \quad (10)$$

We now consider the effect of condensation on isotope ratio. It follows from (10) that $d\ln X_s/dT = -a/T + b/T^2$ for a saturated air parcel. Substituting for $d\ln X_s/dT$ in (5), we derive the result

$$d\ln R/dT = (\alpha - 1)(-a/T + b/T^2) \,. \quad (11)$$

For $\ln\alpha < 1$ we can use the series expansion $\alpha - 1 = \ln\alpha + (\ln\alpha)^2/2 + \cdots$. The lowest-order term is sufficient to provide an accuracy of better than 2% when estimating $\alpha_Q - 1$ at atmospheric temperatures, while we require both the first- and second-order terms to estimate $\alpha_D - 1$ to similar accuracy. After substituting the series expansion for $\alpha - 1$ in (11) and integrating from T_1 to T_2 (where $T_2 < T_1$), we find that

$$R(T_2) = R(T_1) f(T_1, T_2) \,, \quad (12)$$

where when calculating [H_2Q]/[H_2O], we use

$$\ln[f_Q(T_1,T_2)] = -ac_0 \ln(T_2/T_1) + (bc_0 - ac_1)(T_1^{-1} - T_2^{-1}) + (bc_1 - ac_2)(T_1^{-2} - T_2^{-2})/2 + bc_2(T_1^{-3} - T_2^{-3})/3 \,, \quad (13)$$

and when calculating [HDO]/H_2O], we use

$$\ln[f_D(T_1,T_2)] = -ad_0\ln(T_2/T_1) + bd_0(T_1^{-1}-T_2^{-1}) - ad_1(T_1^{-2}-T_2^{-2})/2 + bd_1(T_1^{-3}-T_2^{-3})/3 - ad_2(T_1^{-4}-T_2^{-4})/4 + bd_2(T_1^{-5}-T_2^{-5})/5\,, \quad (14)$$

where $d_0 = c_0(1+c_0/2)$, $d_1 = c_2(1+c_0)$, $d_2 = (c_2)^2/2$, and we have used the fact that $c_1 = 0$ for $\alpha_D(T)$.

Finally, we consider the result of mixing two air parcels with different mixing ratios and isotope ratios. The final mixing ratio X is given by

$$X = gX_i + (1-g)X_j\,, \quad (15)$$

where X_i and X_j are the mixing ratios for parcels i and j, respectively, and g is the fraction of the final parcel derived from parcel i. The final isotope ratio R is given by $R = [gX_iR_i + (1-g)X_jR_j]/X$, where R_i and R_j are the isotope ratios for parcels i and j, respectively. After using (15) to substitute for X, we derive the result

$$R = g'R_i + (1-g')R_j\,, \quad (16)$$

where $g' = gX_i/X$.

If the upper troposphere is not saturated with respect to ice, we can use (8) to estimate the lower stratospheric water vapor mixing ratio (X_{ls}). We assume that the water vapor mixing ratios and isotope ratios in the outflow from conventional and fountain systems are given by $[X_s(T_c), R_s(T_c)]$ and $[X_s(T_f), R_s(T_f)]$, respectively, where T_c and T_f are the temperatures at the tops of conventional and fountain systems, respectively; $X_s(T)$ is given by (10); and $R_s(T) = R_0 f(T_0,T)/\alpha(T_0)$. The mixing ratio in this case is given by

$$X_{ls} = AX_s(T_c) + (1-A)X_s(T_f)\,, \quad (17)$$

where

$$A = \frac{g_u(1-g_f)}{g_d+g_u+g_f(1-g_d-g_u)}\,.$$

By comparing (15)–(16) with (17), we derive the following expression for the lower stratospheric isotope ratio R_{ls}:

$$R_{ls} = A'R_s(T_c) + (1-A')R_s(T_f)\,, \quad (18)$$

where $A' = AX_s(T_c)/X_{ls}$. Equations (17)–(18) show that if the upper troposphere is unsaturated, we expect the composition of the stratosphere to be given by a weighted average of the composition of the outflow from fountains and convective systems, as one might expect if no additional water is removed through condensation.

The mixing ratio in the upper troposphere, X_{ut}, is given by

$$X_{ut} = g_uX_c + g_dX_f + (1-g_u-g_d)X_{ls}\,, \quad (19)$$

where we have assumed that there is no further condensation. If $X_{ut} > X_s(T_t)$, where T_t is the tropopause temperature, then we require that moisture be removed during uplift to maintain saturation over ice and (17)–(18) are no longer valid. The stratospheric mixing ratio in this case is given by

$$X_{ls} = g_fX_s(T_f) + (1-g_f)X_s(T_t)\,. \quad (20)$$

Calculating the isotope ratio when the upper troposphere becomes saturated is more complicated, because the ratio is affected by the Rayleigh fractionation that occurs as excess moisture condenses out during ascent. In this case the isotope ratio at the tropopause is given by $R_{ut}f(T_s,T_t)$, where T_s is defined such that $X_s(T_s) = X_{ut}$ and R_{ut} is the isotope ratio in the upper troposphere before condensation begins. By comparing (15)–(16) with (20), we derive the following expression for the isotope ratio in the lower stratosphere:

$$R_{ls} = BR_s(T_f) + (1-B)R_{ut}f(T_s,T_t)\,, \quad (21)$$

where $B = g_fX_s(T_f)/X_{ls}$. We then compare (15)–(16) with (19) to derive the following expression for R_{ut}:

$$R_{ut} = [g_uX_s(T_c)R_s(T_c) + g_dX_s(T_f)R_s(T_f) + (1-g_d-g_u)X_{ls}R_{ls}]/X_{ut}\,. \quad (22)$$

We use (22) to substitute for R_{ut} in (21) and solve for R_{ls} to derive the result

$$R_{ls} = \frac{[B+(1-B)C_2]R_s(T_f) + (1-B)C_1R_s(T_c)}{1-(1-B)[f(T_s,T_t)-C_1-C_2]}\,, \quad (23)$$

where $C_1 = g_uX_s(T_c)f(T_s,T_t)/X_s(T_s)$ and $C_2 = g_dX_s(T_f)\times f(T_s,T_t)/X_s(T_s)$.

The free parameters in this model include T_0, P_0, T_c, T_f, T_t, Γ, g_f, g_u, g_d, and the ice transition temperature (which determines which functions to use for $e_s(T)$ and $\alpha(T)$). We assume that $\Gamma = 6.646$ K km^{-1}, which is a reasonable approximation in the tropical troposphere. The results of the calculation are not very sensitive to the choice of ice transition temperature, and so we adopt the value 273 K. We set the initial temperature and pressure to 300.5 K and 1013 hPa, respectively, and use the model to calculate solutions after setting the remaining parameters to a variety of values. We show typical results in

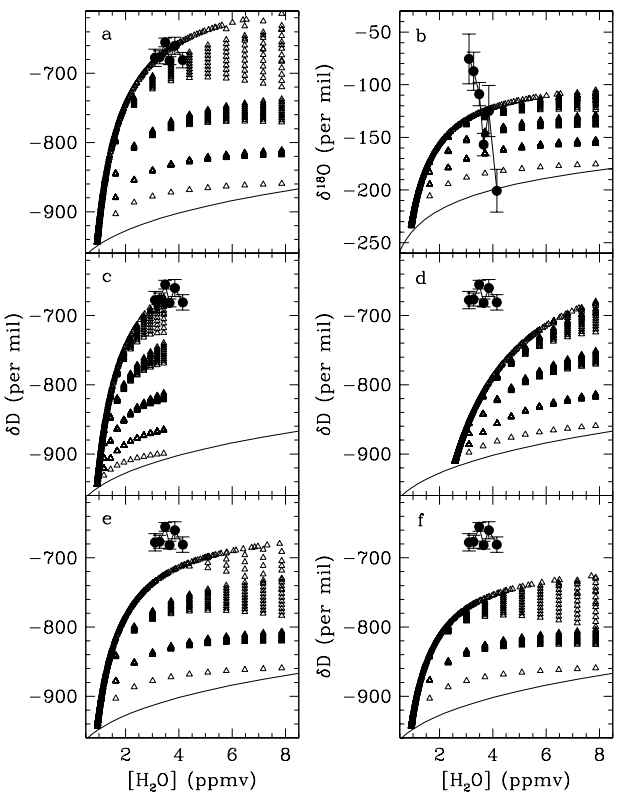

Figure 3. Comparison between measured and modeled [H_2O] and δ in the lower stratosphere. Open triangles represent calculations using the mixed model described in the text; solid circles represent estimates of entry-level composition derived from stratospheric measurements made by FIRS-2 as described by *Johnson et el.* [this issue]. The measurements are binned by [H_2O] before averaging. The calculations in (a) and (b) assume that the heights of the fountain, tropopause, and top of the convective zone are 18, 15.8, and 13 km, respectively, and that the ratio of ice to vapor is 2.8 and 0 in outflow at the base of the convective zone and top of the fountain, respectively (see text). Other panels show calculations for the same set of parameters with the following exceptions: (c) tropopause height increased to 16.7 km; (d) fountain height decreased to 17 km; (e) top of the convective zone increased to 14 km; and (f) ratio of ice to vapor in outflow from the convective zone decreased to 0. Each triangle represents a calculation for a single value for (g_f, g_u, g_d). Each panel shows all results for $0 < g_f < 1$, $0 < g_u < 1$, and $0 < g_d < 1 - g_u$.

Figure 3. Each symbol indicates the result of a single calculation with the model (equations (17)–(18) or (19), (20), and (23), depending on whether or not the upper troposphere becomes saturated) for specific values of T_c, T_f, T_t, g_f, g_u, and g_d. Each panel shows the results when T_c, T_f, and T_t are held constant and g_f, g_u, and g_d are varied over the ranges $0 < g_f < 1$, $0 < g_u < 1$, and $0 < g_d < 1 - g_u$, respectively. Each panel also shows results from the Rayleigh model for a starting temperature of 300.5 K.

We allow for nonzero ice density in convective outflow by first finding z', defined as the altitude at which the saturation mixing ratio is equal to the total water mixing ratio (the sum of vapor and ice) in the outflow. We then assume that convection carries all the vapor from z' to the outflow altitude (some of the water arrives as ice) and mixes with sufficient dry air to evaporate the ice so that no further fractionation occurs. In other words, the result is equivalent to mixing with air transported from z' to the outflow altitude.

All calculations show a similar pattern. The maximum and minimum values for X_{ls} are determined by T_t and T_f, respectively. The calculations are bounded below (most negative δD and δQ) by the Rayleigh model, and the upper bound is determined by the model calculations for values of g_u, g_d, and g_f that do not result in saturation in the upper troposphere. The discrete values of X_{ls} that appear between the upper and lower bounds correspond to the discrete values of g_f used in the calculation, with $g_f = 0$ corresponding to the maximum X_{ls}. The different families of curves running from low to high mixing ratio correspond to different values for g_u, with the splitting resulting from different values for g_d. The most negative values for δD correspond to the largest values for g_u and smallest values for g_d.

4. Comparison With Measurements

We also show in Figure 3 the same estimates of entry-level composition derived from FIRS-2 measurements in the middle stratosphere that were shown in Figure 1, except that the data have been binned by [H_2O] before averaging. The calculation shown in Figures 3a and 3b is consistent with the average measured δD and δQ, although the variation of observed δQ with [H_2O] is not consistent with either the observed dependence of δD with [H_2O] or the calculation. We believe that this is due to the significantly greater sensitivity of measured δQ to errors in [H_2O], resulting from the smaller depletions observed in H_2Q relative to the large depletions observed in HDO. For example, for $(\delta\mathrm{D}, \delta\mathrm{Q}) = (-670‰, -120‰)$, a 5% error

in [H_2O] results in a 42‰ error in δQ but only a 16‰ error in δD. Because the average error in individual [H_2O] measurements is comparable to the bin size used for averaging [see *Johnson et al.*, this issue, Figure 4], the mean [H_2O] for the lowest bin will be biased low by $\sim$ 1 standard deviation, the mean for the highest bin will be biased high by $\sim$ 1 standard deviation, and the bias for other bins will fall in between. We believe that this accounts for the negative slope seen in Figure 3b. Because we consider the measurements of δD to be more robust than the measurements of δQ and because, for the purposes of this comparison, the δQ measurements provide the same information as the δD measurements, the other panels in Figure 3 show only the comparisons between measured and modeled δD.

In Figure 3c we show the result of increasing the tropopause height from 15.8 km (typical for summer) to 16.7 km (typical for winter; the change in altitude is equivalent to reducing the tropopause temperature from 196 to 190 K). The figure looks like a truncated version of Figure 3a, and while it agrees well with the measurements for $[H_2O] < 3.5$ parts per million by volume (ppmv), the reduced tropopause temperature reduces the upper limit for X_{ls}.

Figure 3d shows the effect of reducing the fountain height from 18 km (181 K) to 17 km (188 K). It is important to note that the fountain height is the maximum height reached by the convective system including overshoot and that the air exiting from the top of the fountain does not necessarily stay at that altitude. The fraction of fountain air that stays in the stratosphere is determined by g_f. In this case the model is unable to reproduce the observed δD.

Figure 3e shows the effect of raising the base of the upper troposphere (the altitude above which there is net radiative heating and uplift of air) from 13 km (215 K) to 14 km (208 K), and Figure 3f shows the effect of reducing the ratio of ice to vapor in the outflow of conventional systems from 2.8 (a typical value observed in North Atlantic storm tops [*Smith*, 1992]) to 0. The effect of reducing the amount of ice in the outflow is equivalent in the model to decreasing the temperature (increasing the altitude) of the outflow, as is seen in the figure. The effective temperature for outflow at 13 km with a ratio of ice to vapor of 2.8 is 227.6 K, corresponding to an effective altitude of 11 km. Again, the models are unable to reproduce the observed δD. Increasing the amount of ice in the outflow from convective fountains would have the same effect as reducing the altitude of the fountain outflow, and in all the calculations shown, the density of ice in outflow from fountain systems is set to zero.

In summary, in order to explain the measured δD, we require that air entering the base of the upper troposphere (where radiative uplift begins) comes from convective systems having a maximum effective altitude of 11 km (which can be achieved by convective outflow at 13 km with the ratio of ice to vapor equal to 2.8) and that stratospheric fountains have a minimum effective altitude of 18 km (for example, the maximum altitude reached by overshoot with no ice in the outflow).

We can also place limits on g_f, g_u, and g_d by comparing measured δD as a function of [H_2O] with the calculations in Figures 3a (summer) and 3c (winter). We note that these limits depend on our choice of T_f, T_c, and ice density in the outflow, and so they should be considered as representative rather than absolute. The averaged measurements fall in the range $-682‰ < \delta D < -655‰$, $3.1 \text{ ppmv} < [H_2O] < 4.2$ ppmv. Allowing for an estimated systematic error of 3% in our measurements of [HDO] and [H_2O] increases the range to $-694‰ < \delta D < -641‰$, $3.0 \text{ ppmv} < [H_2O] < 4.3$ ppmv. The calculations that are consistent with the measurements fall in the range $0 < g_f < 0.7$, $0.001 < g_u < 0.032$, and $0.1 < g_d < 0.99$ in summer; and $0 < g_f < 0.16$, $0.001 < g_u < 0.015$, and $0.1 < g_d < 0.99$ in winter. The limits are not entirely independent, and for a given value of one of the variables, the allowed range of the other variables is reduced.

The process can be described qualitatively as follows. The isotopically heavy air at the base of the upper troposphere (amount given by g_u) is mixed with very dry air consisting of subsided air from convective fountains (amount given by g_d) or recycled stratospheric air (amount given by $1 - g_d - g_u$). While most of the air entering the stratosphere comes from the fountain systems (as subsided air and as recirculated stratospheric air), most of the moisture comes from the outflow at the base of the upper troposphere, since the fountain air is so dry. Mixing with air having a water vapor mixing ratio less than the saturation mixing ratio at the average tropopause temperature is the only way to reduce the water vapor mixing ratio to stratospheric values without causing the large depletions in [HDO] that result from condensation and rainout. An important conclusion, also noted by *Moyer et al.* [1996], is that fountain systems cannot be a significant source of moisture in the upper troposphere, since the vapor supplied by convection reaching the tropopause is too depleted in HDO to explain the stratospheric measurements.

Lofting of isotopically heavy ice particles as suggested by *Moyer at al.* [1996] and *Keith* [2000] can increase the abundance of HDO in the upper troposphere and stratosphere, but only if the ice can evaporate into unsaturated

air. Moyer et al. do not identify the source of unsaturated air, while Keith suggests that the air is dehydrated in the same convective events that transport isotopically heavy ice from below 12.5 km (the altitude at which δD in the convective model matches the observed stratospheric value) to the tropopause. The air in the outflow is very dry, with a vapor mixing ratio as low as 0.4 ppmv [*Keith*, 2000], and is subsequently rehydrated by evaporating ice to ~ 4 ppmv as it subsides and the temperature increases. Since the saturation mixing ratio at 12.5 km is 130 ppmv, this process must remove 97% of the water without changing the isotope ratio. We consider it more likely that one system supplies the unsaturated air and another system supplies the water (as ice and vapor), with fountain systems supplying the upper troposphere with dry air that then subsides and is rehydrated by outflow from conventional convective systems.

Our conclusions are consistent with recent studies that find that convective outflow is the dominant source of moisture in the upper troposphere [*Newell et al.*, 1997, *McCormack et al.*, 2000], although it may not seem so at first. These studies have examined tropospheric humidity at 215 hPa (near 12 km) and 147 hPa (near 14 km), the region we refer to as the base of the upper troposphere, and find that convective activity is associated with increased humidity in this region. We also find that the dominant source of moisture in air reaching the stratosphere is convective outflow near the base of the upper troposphere. For this moistening to occur, there needs to be a source of dry air that serves to keep the upper troposphere below saturation in the absence of convective activity. In the present work we find that this air must be very dry to explain our observations of [HDO] in the stratosphere, and the most likely source of sufficiently dry air is deep convection that overshoots the mean tropopause.

The model can be constrained further by considering the distribution of ozone in the upper troposphere. If we assume that the average ozone mixing ratio in the upper troposphere is $< 10\%$ of the mixing ratio in the lower stratosphere (see, for example, the measurements presented by *Vömel et al.* [1995]), then we further require that $< 10\%$ of the air in the upper troposphere consists of recycled stratospheric air. This additional constraint greatly reduces the range for g_d. The calculations for $1 - g_d - g_u < 0.1$ that are also consistent with the measurements fall in the range $0 < g_f < 0.66$, $0.0068 < g_u < 0.032$, and $0.87 < g_d < 0.99$ in summer; and $0 < g_f < 0.16$, $0.0068 < g_u < 0.015$, and $0.89 < g_d < 0.99$ in winter.

5. Conclusion

We conclude that deep convection in the tropics reaches temperatures lower than the mean tropopause temperature and supplies extremely dry air to the upper troposphere. The dry air mixes with uplifted moist air to produce the observed abundance and isotopic composition of stratospheric water vapor. Mixing with dry air is necessary to transport isotopically heavy air from below 11 km to the tropopause without causing larger depletions in HDO than are observed in the stratosphere.

It is important to note that tropopause height, fountain height, and rate of radiative heating in the upper troposphere are not independent parameters, as they have been treated in our model. For example, persistent deep convection can increase the altitude and reduce the temperature of the local tropopause and drive the upper troposphere farther from radiative equilibrium, which will, in turn, affect the heating rate. The heating rate also depends on the abundance of H_2O and O_3, both of which depend on the rates of convection and recirculation of stratospheric air. Proper treatment of all the interactions and feedbacks requires a more sophisticated model than we have presented here. However, our model calculations clearly demonstrate that measurements of the isotopic composition of water vapor provide a powerful tool for exploring transport in the upper troposphere and stratosphere.

Acknowledgments We gratefully acknowledge support from NASA's Upper Atmosphere Research Program in the form of grants NSG 5175 and NAG5-8204. Technical assistance for the balloon flight was provided by the Jet Propulsion Laboratory and the National Scientific Balloon Facility.

References

Brewer, A. W., Evidence for a world circulation provided by the measurements of helium and water vapour distributions in the stratosphere, *Q. J. R. Meteorol. Soc.*, *75*, 351-363, 1949.

Dansgaard, W., Stable isotopes in precipitation, *Tellus*, *16*, 436-468, 1964.

De Bièvre, P., M. Gallet, N. E. Holden, and I. L. Barnes, Isotopic abundances and atomic weights of the elements, *J. Phys. Chem. Ref. Data*, *13*, 809-891, 1984.

Dessler, A. E., E. J. Hintsa, E. M. Weinstock, J. G. Anderson, and K. R. Chan, Mechanisms controlling water vapor in the lower stratosphere: "A tale of two stratospheres," *J. Geophys. Res.100*, 23,167-23,172, 1995.

Irion, F. W., et al., Stratospheric observations of CH_3D and HDO from ATMOS Infrared Solar Spectra: Enrichments of deuterium in methane and implications for HD, *Geophys. Res. Lett.23,* 2381-2384, 1996.

Jancso, G., and W. A. Van Hook, Condensed phase isotope effects (especially vapor pressure isotope effects), *Chem. Rev. Washington D. C., 74,* 689-750, 1974.

Jensen, E. J., W. G. Read, J. Mergenthaler, B. J. Sandor, L. Pfister, and A. Tabazadeh, High humidities and subvisible cirrus near the tropical tropopause, *Geophys. Res. Lett.26,* 2347-2350, 1999.

Johnson, D. G., K. W. Jucks, W. A. Traub, and K. V. Chance, Smithsonian stratospheric far-infrared spectrometer and data reduction system, *J. Geophys. Res.100,* 3091-3106, 1995.

Johnson, D. G., K. W. Jucks, W. A. Traub, and K. V. Chance, Isotopic composition of stratospheric water vapor: Measurements and photochemistry, *J. Geophys. Res.*this issue.

Jouzel, J., and L. Merlivat, Deuterium and oxygen 18 in precipitation: Modeling of the isotopic effects during snow formation, *J. Geophys. Res.89,* 11,749-11,757, 1984.

Keith, D. W., Stratosphere-troposphere exchange: Inferences from the isotopic composition of water vapor, *J. Geophys. Res.105,* 15,167-15,173, 2000.

McCormack, J. P., R. Fu, and W. G. Read, The influence of convective outflow on water vapor mixing ratios in the tropical upper troposphere: An analysis based on UARS MLS measurements, *Geophys. Res. Lett.27,* 525-528, 2000.

Merlivat, L., and G. Nief, Fractionnement isotopique lors des changements d'état solide-vapeur et liquide-vapeur de l'eau à des températures inférieures à 0°C, *Tellus, 19,* 122-127, 1967.

Moyer, E. J., F. W. Irion, Y. L. Yung, and M. R. Gunson, ATMOS stratospheric deuterated water and implications for troposphere-stratosphere transport, *Geophys. Res. Lett.23,* 2385-2388, 1996.

Newell, R. E., and S. Gould-Stewart, A stratospheric fountain?, *J. Atmos. Sci, 38,* 2789-2796, 1981.

Newell, R. E., Y. Zhu, W. G. Read, and J. W. Waters, Relationship between upper tropospheric moisture and eastern tropical Pacific sea surface temperature at seasonal and interannual time scales, *Geophys. Res. Lett.24,* 25-28, 1997.

Press, W. H., S. A. Teukolsky, W. T. Vetterling, and B. P. Flannery, *Numerical Recipes in Fortran: The Art of Scientific Computing,* 2nd ed., Cambridge Univ. Press, New York, 1992.

Sherwood, S. C., and A. E. Dessler, On the control of stratospheric humidity, *Geophys. Res. Lett.27,* 2513-2516, 2000.

Smith, R. B., Deuterium in North Atlantic storm tops, *J. Atmos. Sci., 49,* 2041-2057, 1992.

Smithsonian Institution, Smithsonian Meteorological Tables, 6th rev. ed., *Smithson. Misc. Collect., 114,* 527 pp., 1951.

Vömel, H., S. J. Oltmans, D. Kley, and P. J. Crutzen, New evidence for the stratospheric dehydration mechanism in the equatorial Pacific, *Geophys. Res. Lett.22,* 3235-3238, 1995.

Zahn, A., V. Barth, K. Pfeilsticker, and U. Platt, Deuterium, oxygen 18, and tritium as tracers for water vapour transport in the lower stratosphere and tropopause region, *J. Atmos. Chem., 30,* 25-47, 1998.

This preprint was prepared with the AGU LaTeX macros v3.1. File h2otrop formatted 2001 May 3.